Inorg. Chem. **2008**, *47*, 4243−4255

A New Class of Luminescent Tricarbonyl Rhenium(I) Complexes Containing Bridging 1,2-Diazine Ligands: Electrochemical, Photophysical, and Computational Characterization

Daniela Donghi,[†] Giuseppe D'Alfonso,[*,†,⊥,#] Matteo Mauro,[†] Monica Panigati,[†] Pierluigi Mercandelli,[*,⊥,#,‡] Angelo Sironi,[⊥,#,‡] Patrizia Mussini,[*,⊥,§] and Laura D'Alfonso[||]

Dipartimento di Chimica Inorganica, Metallorganica e Analitica (DCIMA), Università di Milano, via Venezian 21, I-20133 Milano, Italy, Dipartimento di Chimica Strutturale e Stereochimica Inorganica (DCSSI), Università di Milano, via Venezian 21, I-20133 Milano, Italy, Dipartimento di Chimica Fisica ed Elettrochimica (DCFE), Università di Milano, via Golgi 19, I-20133 Milano, Italy, Dipartimento di Fisica, Università di Milano-Bicocca, piazza della Scienza 6, I-20126 Milano, Italy, Centro di Eccellenza CIMaINa, Università di Milano, via Venezian 21, I-20133 Milano, Italy, and Istituto di Scienze e Tecnologie Molecolari (ISTM) del CNR, via Venezian 21, I-20133 Milano, Italy

Received December 5, 2007

A novel class of luminescent tricarbonyl rhenium(I) complexes of general formula $[Re_2(\mu\text{-}X)_2(CO)_6(\mu\text{-diaz})]$ (X = halogen and diaz = 1,2-diazine) was prepared by reacting $[ReX(CO)_5]$ with 0.5 equiv of diazine (seven different ligands were used). The bridging coordination of the diazine in these dinuclear complexes was confirmed by single-crystal X-ray analysis. Cyclic voltammetry in acetonitrile showed for all the complexes (but the phthalazine derivative) a chemically and electrochemically reversible ligand-centered reduction, as well as a reversible metal-centered bielectronic oxidation. With respect to the prototypical luminescent $[ReCl(CO)_3(bpy)]$ complex, the oxidation is more difficult and the reduction easier (about +0.3 V), so that a similar highest occupied molecular orbital–lowest unoccupied molecular orbital gap is observed. All of the complexes exhibit photoluminescence at room temperature in solution, with broad unstructured emission from metal-to-ligand charge-transfer states, at λ in the range 579–620 nm. Lifetimes (τ = 20–2200 ns) and quantum yields (Φ up to 0.12) dramatically change upon varying the bridging ligand X and the diazine substituents: in particular, quantum yields decrease in the series Cl, Br, and I and in the presence of substituents at the α positions of the pyridazine ring. A combined density functional and time-dependent density functional study of the geometry, relative stability, electronic structure, and photophysical properties of all the pyridazine derivatives was performed. The nature of the excited states involved in the electronic absorption spectra was ascertained, and trends in the energy of the highest occupied and lowest unoccupied molecular orbitals upon changing the pyridazine substituents and the bridging halogen ligands were discussed. The observed emission properties of these complexes were shown to be related to a combination of steric and electronic factors affecting their ground-state geometry and their stability.

Introduction

After more than three decades from the pioneer studies on the excited states of rhenium(I) diimine tricarbonyl complexes,[1] the interest toward the photochemical and photophysical properties of these complexes is far from being on a decline, due to their broad range of applications. These include photoredox chemistry,[2] chemi- or electrochemiluminescence,[3] chemical and biological sensing,[4,5] and bio-

* To whom correspondence should be adressed. E-mail: giuseppe.dalfonso@unimi.it (G.D.); pierluigi.mercandelli@unimi.it (P.M.); patrizia.mussini@unimi.it (P.M.).
† DCIMA Milano.
‡ DCSSI Milano.
§ DCFE Milano.
|| Università di Milano-Bicocca.
⊥ CIMaINa Milano.
ISTM Milano.

(1) Wrighton, M.; Morse, D. L. *J. Am. Chem. Soc.* **1974**, *96*, 998–1003.
(2) (a) See for instance: Tsubaki, H.; Sekine, A.; Ohashi, Y.; Koike, K.; Takeda, H.; Ishitani, O. *J. Am. Chem. Soc.* **2005**, *127*, 15544–15555. (b) Gibson, D. H.; He, H. *Chem. Commun.* **2001**, 2082–2083, and refs therein. (c) See also: Kalyanasundaram, K. *J. Chem. Soc., Faraday Trans. 2* **1986**, *82*, 2401–2415.
(3) Richter, M. M. *Chem. Rev.* **2004**, *101*, 3003–3036.

10.1021/ic7023692 CCC: $40.75
Published on Web 04/19/2008

conjugation.[6] Recently, several papers have appeared dealing with their use as phosphorescent dopants for organic light-emitting diodes (OLED),[7] and also as electroluminescent emitters in single-layer OLED devices.[8]

The complexes initially investigated were mononuclear species containing chelating diimine ligands, of general formula *fac*-$[ReX(CO)_3(N\text{-}N)]^{n+}$ (*N-N* = 1,10-phenanthroline or 2,2′-bipyridine, X anionic, typically halide, or neutral monodentate ligand, with $n = 0$ or 1, respectively).[9–15] Like other d^6 transition metal complexes, these species exhibit intense and unstructured emission in fluid solution, originating from $d\pi(Re)-\pi^*(N\text{-}N)$ metal-to-ligand charge-transfer (MLCT) excited states that are mainly of triplet character (even if the large spin–orbital coupling in third-row transition metals precludes discrete singlet and triplet states). Subsequently, also polynuclear luminescent complexes, usually constituted by octahedral $ReX(CO)_3$ corners connected by bridging 1,4-diazines or bipyridines, have been characterized.[5,16–20]

We have recently reported the synthesis and a preliminary photophysical characterization of a different kind of polynuclear luminescent $Re(CO)_3$ derivative,[21] isolated from the reaction of the unsaturated tetrahedral hydridocarbonyl cluster $[Re_4(\mu\text{-}H)_4(CO)_{12}]$ with 1,2-diazines (pyridazine or phthalazine). These species were the dinuclear complexes $[Re_2(\mu\text{-}H)_2(CO)_6(\mu\text{-diaz})]$ (diaz = 1,2-diazine) and the square

(4) (a) Beck, D.; Brewer, J.; Lee, J.; McGraw, D.; DeGraff, B. A.; Demas, J. N. *Coord. Chem. Rev.* **2007**, *251*, 546–553. (b) Sathiyendiran, M.; Liao, R.-T.; Thanasekaran, P.; Luo, T.-T.; Venkataramama, N. S.; Lee, G.-H.; Peng, S.-M.; Lu, K.-L. *Inorg. Chem.* **2006**, *45*, 10052–10054. (c) Wong, K. M.-C.; Li, W.-P.; Cheung, K.-K.; Yam, V. W.-W. *New. J. Chem.* **2005**, *29*, 165–172. (d) Huynh, L.; Wang, Z.; Yang, J.; Stoeva, V.; Lough, A.; Manners, I.; Winnik, M. A. *Chem. Mater.* **2005**, *17*, 4765–4773. (e) Bare, W. D.; Mack, N. H.; Xu, W.; Demas, J. N. *Anal. Chem.* **2002**, *74*, 2198–2209. (f) Lee, S. J.; Lin, W. *J. Am. Chem. Soc.* **2002**, *124*, 4554–4555. (g) Uppadine, L. H.; Keene, F. R.; Beer, P. D. *J. Chem. Soc., Dalton Trans.* **2001**, 2188–2198. (h) Cooper, J. B.; Drew, M. G. B.; Beer, P. D. *J. Chem. Soc., Dalton Trans.* **2000**, 2721–2728. (i) Beer, P. D.; Tomoshenko, V.; Maestri, M.; Passaniti, P.; Balzani, V. *Chem. Commun* **1999**, 1755–1756.

(5) (a) Blanco-Rodriguez, A. N.; Busby, M.; Gradinaru, C.; Crane, B. R.; Di Bilio, A. J.; Matousek, P.; Towrie, M.; Leigh, B. S.; Richards, J. H.; Vlček, A., Jr; Gray, H. B. *J. Am. Chem. Soc.* **2006**, *128*, 4365–4370. (b) Lo, K. K.-W.; Tsang, K. H.-K.; Sze, K.-S. *Inorg. Chem.* **2006**, *45*, 1714–1722. (c) Guo, X.-Q.; Castellano, F. N.; Lakowicz, J. R. *Anal. Chem.* **1988**, *70*, 632–637.

(6) (a) For same recent papers, see: James, S.; Maresca, K. P.; Babich, J. W.; Valliant, J. F.; Doering, L.; Zubieta, J. *Bioconjugate Chem.* **2006**, *17*, 590–596. (b) Lo, K. K.-W.; Tsang, K. H.-K.; Zhu, N. *Organometallics* **2006**, *25*, 3220–3227. (c) Reece, S. J.; Seyedsayamdost, M. R.; Stubbe, J.; Nocera, D. G. *J. Am. Chem. Soc.* **2006**, *128*, 13654–13655. (d) Lo, K. K.-W.; Hui, W.-K.; Chung, C.-K.; Tsang, K. H.-K.; Lee, T. K.-M.; Li, C.-K.; Lau, J. S.-Y.; Ng, D. C.-M. *Coord. Chem. Rev.* **2006**, *250*, 1724–1736. (e) Lo, K. K.-W.; Hui, W.-K.; Chung, C.-K.; Tsang, K. H.-K.; Ng, D. C.-M.; Zhu, N.; Cheung, K.-K. *Coord. Chem. Rev.* **2005**, *249*, 1434–1450. (f) Lo, K. K.-W.; Tsang, K. H.-K.; Zhu, N. *Inorg. Chem.* **2005**, *44*, 6100–6110. (g) Wei, L.; Babich, J.; Eckelman, W. C.; Zubieta, J. *Inorg. Chem.* **2005**, *44*, 2198–2209. (h) Di Bilio, A. J.; Crane, B. R.; Wehbi, W. A.; Kiser, C. N.; Abu-Omar, M. M.; Carlos, R. M.; Richards, J. H.; Winkler, J. R.; Gray, H. B. *J. Am. Chem. Soc.* **2001**, *123*, 3181–3182.

(7) (a) Liu, C.; Li, J.; Li, B.; Hong, Z. R.; Zhao, F. F.; Liu, S. Y.; Li, W. L. *Chem. Phys. Lett.* **2007**, *435*, 54–58. (b) Liu, C.; Li, J.; Li, B.; Hong, Z.; Zhao, F.; Liu, S.; Li, W. *Appl. Phys. Lett.* **2006**, *89*, 243511. (c) Fu, C.; Li, M.; Su, Z.; Hong, Z.; Li, W.; Li, B. *Appl. Phys. Lett.* **2006**, *88*, 093507. (d) Lundin, N. J.; Blackman, A. G.; Gordon, K. C.; Officer, D. L. *Angew. Chem., Int. Ed.* **2006**, *45*, 2582–2584. (e) Duan, Y.; Li, J.; Zhao, Y.; Cheng, G.; Hou, J.; Liu, S. *Opt. Quant. Electron.* **2005**, *37*, 1121–1127. (f) Li, B.; Li, M.; Hong, Z.; Li, W.; Yu, T.; Wei, H. *Appl. Phys. Lett.* **2004**, *85*, 4786–4788. (g) Wong, H. L.; Lam, L. S. M.; Cheng, K. W.; Man, K. Y. K.; Chan, W. K. *Appl. Phys. Lett.* **2004**, *84*, 2557–2559. (h) Li, F.; Zhang, M.; Cheng, G.; Feng, J.; Zhao, Y.; Ma, Y.; Liu, S.; Shen, J. *Appl. Phys. Lett.* **2004**, *84*, 148–150. (i) Li, F.; Cheng, G.; Zhao, Y.; Feng, J.; Liu, S.; Zhang, M.; Ma, Y.; Shen, J. *Appl. Phys. Lett.* **2003**, *83*, 4716–4718. (j) Li, F.; Zhang, M.; Feng, J.; Cheng, G.; Wu, Z.; Ma, Y.; Liu, S. *Appl. Phys. Lett.* **2003**, *83*, 365–367. (k) Ranjan, S.; Lin, S.-Y.; Hwang, K.-C.; Chi, Y.; Ching, W.-L.; Liu, C.-S.; Tao, Y.-T.; Chien, C.-H.; Peng, S.-M.; Lee, G.-H. *Inorg. Chem.* **2003**, *42*, 1248–1255. (l) Wang, K.; Huang, L.; Gao, L.; Jin, L.; Huang, C. *Inorg. Chem.* **2002**, *41*, 3353–3358. (m) Li, Y.; Liu, Y.; Guo, J.; Wu, F.; Tian, W.; Li, B.; Wang, Y. *Synth. Met.* **2001**, *118*, 175–179.

(8) (a) Yam, V. W.-W.; Li, B.; Yang, Y.; Chu, B. W.-K.; Wong, K. M.-C.; Cheung, K.-K. *Eur. J. Inorg. Chem.* **2003**, 4035–4042. (b) Chan, W. K.; Ng, P. K.; Gong, X.; Hou, S. *Appl. Phys. Lett.* **1999**, *75*, 3920–3922. (c) Gong, X.; Ng, K.; Chan, W. K. *Adv. Mater.* **1998**, *10*, 1337–1340.

(9) (a) For early works, see refs.10−13 For some more recent work, see refs.14 and 15 For pertinent reviews see: Striplin, D. R.; Crosby, G. A. *Coord. Chem. Rev.* **2001**, *211*, 163–175. (b) Stukfens, D. J., Jr.; Vlcek, A. *Coord. Chem. Rev.* **1998**, *177*, 127–179. (c) Lees, A. J. *Coord. Chem. Rev.* **1998**, *177*, 3–35. (d) Schanze, K. S.; MacQueen, D. B.; Perkins, T. A.; Cabana, L. A. *Coord. Chem. Rev.* **1993**, *122*, 63–89. (e) Lees, A. J. *Chem. Rev.* **1987**, *87*, 711–743.

(10) (a) Giordano, P. J.; Fredericks, S. M.; Wrighton, M. S.; Morse, D. L. *J. Am. Chem. Soc.* **1978**, *100*, 2257–2259. (b) Luong, J. C.; Nadjo, L.; Wrighton, M. S. *J. Am. Chem. Soc.* **1978**, *100*, 5790–5795. (c) Fredericks, S. M.; Luong, J. C.; Wrighton, M. S. *J. Am. Chem. Soc.* **1979**, *101*, 7415–7417. (d) Smothers, W. K.; Wrighton, M. S. *J. Am. Chem. Soc.* **1983**, *105*, 1067–1069.

(11) (a) Caspar, J. V.; Meyer, T. J. *J. Phys. Chem.* **1983**, *87*, 952–957. (b) Caspar, J. V.; Westmoreland, T. D.; Allen, G. H.; Bradley, P. G.; Meyer, T. J.; Woodruff, W. H. *J. Am. Chem. Soc.* **1984**, *106*, 3492–3500. (c) Caspar, J. V.; Sullivan, C. B.; Meyer, T. J. *Inorg. Chem.* **1984**, *23*, 2104–2109.

(12) Juris, A.; Campagna, S.; Bidd, S.; Lehn, J.-M.; Ziessel, R. *Inorg. Chem.* **1988**, *27*, 4007–4011.

(13) (a) Sacksteder, L.; Zipp, A. P.; Brown, E. A.; Streich, J.; Demas, J. N.; DeGraff, B. A. *Inorg. Chem.* **1990**, *29*, 4335–4340. (b) Sacksteder, L.; Lee, M.; Demas, J. N.; DeGraff, B. A. *J. Am. Chem. Soc.* **1993**, *115*, 8230–8238.

(14) (a) Lee, P. H.-M.; Ko, C.-C.; Zhu, N.; Yam, V. W.-W. *J. Am. Chem. Soc.* **2007**, *129*, 6058–6059. (b) Ko, C.-C.; Kwok, W.-M.; Yam, V. W.-W.; Phillips, D. L. *Chem.—Eur. J.* **2006**, *12*, 5840–5848. (c) Yam, V. W.-W.; Ko, C.-C.; Zhu, N. *J. Am. Chem. Soc.* **2004**, *126*, 12734–12735. (d) Ko, C.-C.; Wu, L.-X.; Wong, K. M.-C.; Zhu, N.; Yam, V. W.-W. *Chem.—Eur. J.* **2004**, *10*, 766–776. (e) Yam, V. W.-W.; Yang, Y.; Zhang, J.; Chu, B. W.-K.; Zhu, N. *Organometallics* **2001**, *20*, 4911–4918. (f) Yam, V. W.-W. *Chem. Commun.* **2001**, 789–796.

(15) (a) Villegas, J. M.; Stoyanov, S. R.; Huang, W.; Rillema, D. P. *Dalton Trans.* **2005**, 1042–1051. (b) Villegas, J. M.; Stoyanov, S. R.; Huang, W.; Rillema, D. P. *Inorg. Chem.* **2005**, *44*, 2297–2309.

(16) (a) Dinolfo, P. H.; Hupp, J. T. *J. Am. Chem. Soc.* **2004**, *126*, 16814–16819. (b) Dinolfo, P. H.; Williams, M. E.; Stern, C. L.; Hupp, J. T. *J. Am. Chem. Soc.* **2004**, *126*, 12989–13001. (c) Bélanger, S.; Hupp, J. T.; Stern, C. L.; Slone, R. V.; Watson, D. F.; Carrel, T. G. *J. Am. Chem. Soc.* **1999**, *121*, 557–563. (d) Slone, R. V.; Benkstein, K. D.; Bélanger, S.; Hupp, J. T.; Guzei, I. A.; Rheingold, A. L. *Coord. Chem. Rev.* **1998**, *171*, 221–243.

(17) (a) Sun, S.-S.; Lees, A. J. *Organometallics* **2002**, *21*, 39–49. (b) Sun, S.-S.; Lees, A. J. *J. Am. Chem. Soc.* **2000**, *122*, 8956–8967.

(18) (a) Sathieyendiran, M.; Liao, R.-T.; Thanasekaran, P.; Luo, T.-T.; Venkataramanan, N. S.; Lee, G.-H.; Peng, S.-M.; Lu, K.-L. *Inorg. Chem.* **2006**, *45*, 10052–10054. (b) Thanasekaran, P.; Liao, R.-T.; Liu, Y.-H.; Rajagopal, S.; Rajendran, T.; Lu, K.-L. *Coord. Chem. Rev.* **2005**, *249*, 1085–1110. (c) Rajendran, T.; Manimaran, B.; Liao, R.-T.; Lin, R.-J.; Thanasekaran, P.; Lee, G.-H.; Peng, S.-M.; Liu, Y.-H.; Chang, I.-J.; Rajagopal, S.; Lu, K.-L. *Inorg. Chem.* **2003**, *42*, 6388–6394. (d) Manimaran, B.; Thanasekaran, P.; Rajendran, T.; Liao, R.-T.; Liu, Y.-H.; Lee, G.-H.; Peng, S.-M.; Rajagopal, S.; Lu, K.-L. *Inorg. Chem.* **2003**, *42*, 4795–4797. (e) Rajendran, T.; Manimaran, B.; Lee, F.-Y.; Lee, G.-H.; Peng, S.-M.; Wang, C.-M.; Lu, K.-L. *Inorg. Chem.* **2000**, *39*, 2016–2017.

(19) Ortiz, T. P.; Marshall, J. A.; Emmert, L. A.; Yang, J.; Choi, W.; Costello, A. L.; Brozik, J. A. *Inorg. Chem.* **2004**, *43*, 132–141.

(20) See also the unusual linear-shaped trimers and tetramers, containing Re(CO) *n*(bpy) centers ($n = 2, 3$), reported by Ishitani, O.; Kanai, K.; Yamada, Y.; Sakamoto, K. *Chem. Commun.* **2001**, 1514–1515.

(21) Panigati, M.; Donghi, D.; D'Alfonso, G.; Mercandelli, P.; Sironi, A.; D'Alfonso, L. *Inorg. Chem.* **2006**, *26*, 10909–10921.

Scheme 1

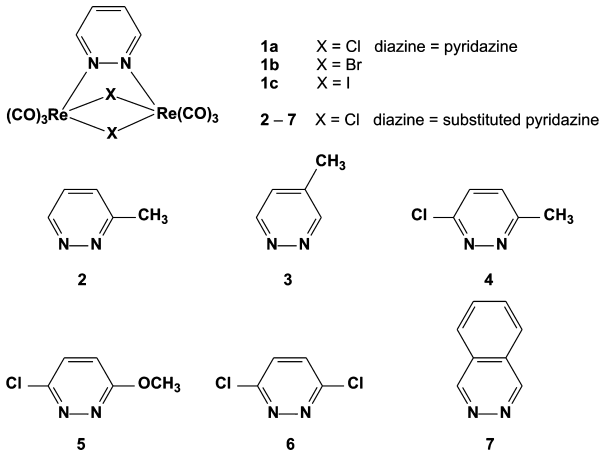

clusters $[Re_4(\mu\text{-}H)_4(CO)_{12}(\mu\text{-diaz})_2]$, formally dimers of the previous ones. The latter showed emission in the range 580–611 nm, with fair (>0.01) quantum yields, while the emitting properties of the dinuclear species were much poorer ($\Phi \approx 0.001$, at 590–645 nm).

To the best of our knowledge, this was the first report of luminescence arising from a MLCT transition involving a 1,2-diazine. Few examples of transition metal complexes containing 1,2-diazines are present in the literature. This is probably due to their steric and electronic properties, which seem to be unfavorable compared to the typical diimine ligands, such as phenanthroline and bipyridine. Indeed, in 1,2-diazines, the orientation of the nitrogen lone pairs does not allow chelation on a single metal center. Moreover, the presence of two nitrogen atoms on the same aromatic ring makes diazines electron-poorer (hence with a lower σ-donor ability) than bipyridines. On the other hand, these electronic factors should favor ligand reduction in the metal-to-ligand charge transfer. Furthermore, the orientation of the nitrogen lone pairs allows bridging coordination on suitable metal fragments.

We have therefore decided to investigate the properties of 1,2-diazines as bridging ligands toward a dinuclear $Re_2(\mu\text{-}X)_2(CO)_6$ core, where X is a halide (Cl, Br, and I). We report here on the synthesis and photophysical characterization of a series of $[Re_2(\mu\text{-}X)_2(CO)_6(\mu\text{-diaz})]$ complexes, in which the pyridazine ring contains different substituents, in order to modulate the electronic and steric properties of the ligand. The highest occupied molecular orbital–lowest unoccupied molecular orbital (HOMO–LUMO) gaps of the complexes have been determined by cyclic voltammetry (CV). The nature of the frontier orbitals and the properties of the excited states have been investigated by density functional and time-dependent density functional calculations. The obtained results, in particular the high quantum yields exhibited by some of the new complexes, lead us to conclude that this new class of photoluminescent species deserves further work along the lines suggested by the theoretical study.

Results and Discussion

Synthesis of the New Complexes. The $[Re_2(\mu\text{-}X)_2(CO)_6(\mu\text{-diaz})]$ derivatives shown in Scheme 1 were cleanly obtained in high isolated yields (60–80%) by treating the $[ReX(CO)_5]$ complexes (X = Cl, Br, and I) with 0.5 equiv of the corresponding 1,2-diazine, in toluene at reflux, according to eq 1.[22] The good selectivity of the synthesis was attested to by spectroscopic analyses (IR and NMR) of the reaction mixtures. All of the products exhibited four ν(CO) bands, as the analogous hydridic derivatives $[Re_2(\mu\text{-}H)_2(CO)_6(\mu\text{-diaz})]$.[21]

$$2[ReX(CO)_5] + \text{diaz} \rightarrow [Re_2(\mu\text{-}X)_2(CO)_6(\mu\text{-diaz})] + 4CO \quad (1)$$

The new complexes can be obtained also by reacting equimolar amounts of the diazine and of the dinuclear complexes $[Re_2(\mu\text{-}X)_2(CO)_8]$ (eq 2), as was checked for the pyridazine (pydz) derivative.

$$[Re_2(\mu\text{-}X)_2(CO)_8] + \text{pydz} \rightarrow [Re_2(\mu\text{-}X)_2(CO)_6(\mu\text{-pydz})] + 2CO \quad (2)$$

All of the complexes are thermally stable in nondonor solvents. In the donor solvent acetonitrile, used for cyclovoltammetric characterization, complexes **4**–**6** underwent rapid fragmentation with the loss of the diazine ligand, according to eq 3 (with $t_{1/2}$ values ranging from a few minutes to a few hours, as detailed in the following). Such complexes are those for which the lowest values of interaction energy have been computed (see Table 1 below).

$$[Re_2(\mu\text{-}Cl)_2(CO)_6(\mu\text{-diaz})] + 2\text{MeCN} \rightarrow 2[ReCl(CO)_3(MeCN)_2] + \text{diaz} \quad (3)$$

The structure of the complexes has been established by single-crystal X-ray analysis of the $[Re_2(\mu\text{-}Cl)_2(CO)_6(\mu\text{-pydz})]$ derivative **1a**.[23] Figure 1 shows a picture of **1a** along with some relevant geometrical parameters, averaged according to the idealized C_{2v} symmetry of this molecule. Each rhenium atom attains a distorted octahedral coordination and bears three terminal carbonyl ligands (in a facial arrangement), two bridging chloro ligands, and one of the nitrogen atoms of the bridging pyridazine ligand. The molecular structure of **1a** is strictly related to that of the corresponding chloro-carbonyl derivative $[Re_2(\mu\text{-}Cl)_2(CO)_8]$.[24] The bridging coordination of a pyridazine molecule leads, however, to major perturbation of the structure. Indeed, to allow the lone pairs on the two nitrogen atoms to effectively interact with the metal atoms, the two rhenium-centered octahedra must bend toward the bridging ligand, leading to a larger Re···Re−C(axial) angle (+26.9°) and to a shorter Re···Re distance (−27.3 pm) with respect to the D_{2h}-symmetric chloro-carbonyl species.

(22) The reaction between pyridazine and $[ReX(CO)_5]$ (X = Cl, Br, and I) had been previously investigated using an excess of the ligand, leading to stable derivatives of formula *fac*-$[ReX(CO)_3(pydz)_2]$ containing two monodentate diazines. The photophysical properties of these species had not been investigated: Abel, E. W.; Blackwall, E. S.; Heard, P. J.; Orrel, K. G.; Sik, V.; Hursthouse, M. B.; Mazid, A. M.; Abdul Malik, K. M. *J. Chem. Soc., Dalton Trans.* **1994**, *100*, 445–455.

(23) CCDC-655526 contains the crystallographic data for **1a**. These data can be obtained free of charge from The Cambridge Crystallographic Data Centre (www.ccdc.cam.ac.uk; accessed Mar 2008).

(24) Vega, A.; Calvo, V.; Manzur, J.; Spodine, E.; Saillard, J.-Y. *Inorg. Chem.* **2002**, *41*, 5382–5387.

Table 1. Computed Interaction Energies (E_{int}), Ligand Repulsion Energies (E_r), Charge Transfers (q[Re_2]), HOMO–LUMO Gaps, and Electronic Transition Energies for the [$Re_2(\mu$-X$)_2(CO)_6(\mu$-diaz)] Complexes

	μ-diaz	μ-X	E_{int}[a] [kJ mol^{-1}]	E_r[b] [kJ mol^{-1}]	q[Re_2][c]	$\Delta E_{HOMO-LUMO}$ [eV]	λ_{abs}[d] [nm, eV] (f)	λ_{abs}[e] [nm, eV] (f)
1a	pydz	Cl	0	0	−0.308	3.32	385, 3.22 (0.14)	370, 3.35 (0.21)
1b	pydz	Br	−9	13	−0.302	3.27	384, 3.23 (0.14)	370, 3.35 (0.20)
1c	pydz	I	−16	30	−0.288	3.17	384, 3.23 (0.10)	371, 3.34 (0.20)
	3,6-Me_2pydz	Cl	−13	786	−0.324	3.52	373, 3.32 (0.14)	355, 3.49 (0.18)
	4,5-Me_2pydz	Cl	11	−2	−0.335	3.51	372, 3.34 (0.19)	355, 3.49 (0.25)
6	3,6-Cl_2pydz	Cl	−64	207	−0.283	2.94	426, 2.91 (0.13)	404, 3.07 (0.19)
	4,5-Cl_2pydz	Cl	−21	−5	−0.289	3.18	396, 3.13 (0.18)	390, 3.18 (0.26)
2	3-Mepydz	Cl	−7	315	−0.319	3.42	380, 3.26 (0.15)	364, 3.41 (0.20)
3	4-Mepydz	Cl	6	−2	−0.322	3.41	380, 3.27 (0.17)	364, 3.41 (0.23)
4	3-Cl-6-Mepydz	Cl	−40	484	−0.304	3.20	399, 3.11 (0.14)	378, 3.28 (0.18)
5	3-Cl-6-OMepydz	Cl	−34	187	−0.283	3.02	415, 2.99 (0.17)	394, 3.15 (0.22)

[a] Values are relative to E_{int} (**1a**) = 283 kJ mol^{-1}. [b] Values are relative to E_r (**1a**) = 128 kJ mol^{-1}. [c] Sum of the natural charges of the $Re_2(\mu$-X$)_2(CO)_6$ moiety. [d] Gas-phase values. [e] Toluene solution values (CPCM). The values of the $a_2 \rightarrow a_2$ transition are given. For a list of all the transitions with $f > 0.01$ see Table S4 (Supporting Information).

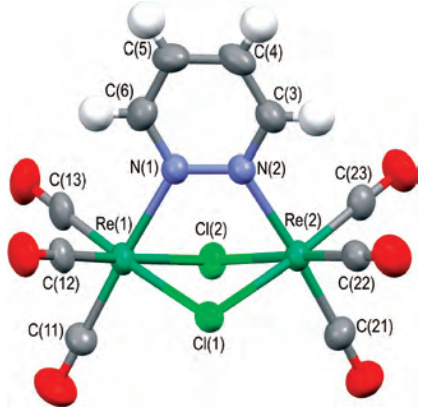

Figure 1. View of the [$Re_2(\mu$-Cl$)_2(CO)_6(\mu$-pydz-κN^1:κN^2)] (**1a**) molecule with a partial labeling scheme. Average bond distances [pm] and angles [deg]: Re···Re 354.11(8), Re−Cl 249.9(6), Re−N 220.5(6), N−N 135.3(6), Cl−Re−Cl 81.27(13), Re−N−N 119.6(16), Re···Re−C(axial) 116.2(17). Further geometrical parameters are listed in the Supporting Information.

Electrochemical Characterization. The complexes **1–7** and the corresponding free ligands (labeled $\mathbf{L_n}$, where n refers to the numbers in Scheme 1) have been investigated by CV, in order to evidence the changes induced by coordination.

Ligands. All free ligands feature only reduction peaks (either a single one or a peak combination) in the potential window available in the chosen medium, that is, acetonitrile (hereafter MeCN) containing 0.1 M tetrabutylammonium hexafluorophosphate ($TBAPF_6$). Looking at the synopsis of the relevant CV characteristics (Figure 2) and relevant parameters (Table 2), the first reduction peak appears to be chemically irreversible, excepting phthalazine ($\mathbf{L_7}$). The latter shows a chemically and electrochemically reversible peak, as implied by the half-peak width and the nearly zero slope of the E_p versus log v linear characteristics (where v indicates the scan rate). This is consistent with the enhanced stabilization provided to the charged radical anion intermediate by the π system including the phenyl ring condensed on the pyridazine one.

The normalized limiting current density after peak convolution[25] is consistent with a monoelectronic stoichiometry for $\mathbf{L_7}$ (see Table 2) while it is consistent with a bielectronic stoichiometry for the first reduction peak of $\mathbf{L_1}$–$\mathbf{L_6}$ (taking into account the decrease of the diffusion coefficient with increasing ring substitution).

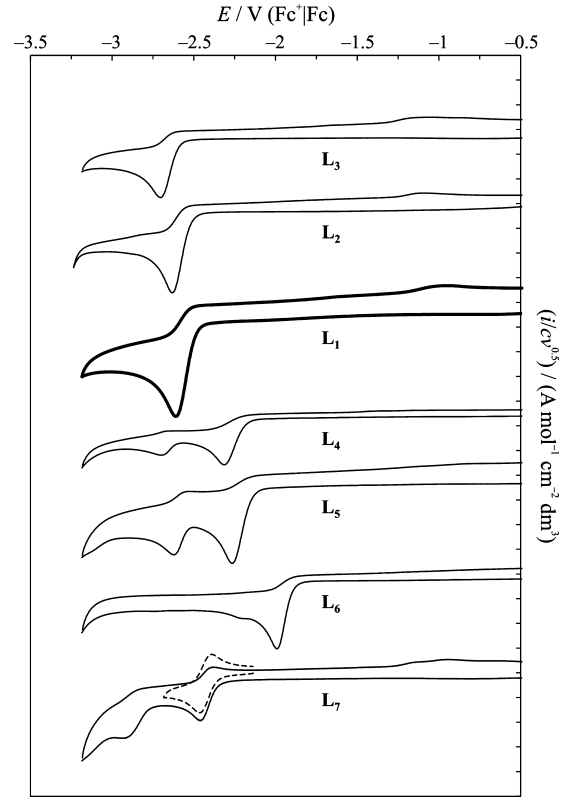

Figure 2. A synopsis of CV characteristics obtained for the free ligands $\mathbf{L_n}$, at a 0.2 V s^{-1} scan rate, in MeCN, with 0.1 M $TBAPF_6$ as the supporting electrolyte, at 298 K, with ohmic drop compensation.

Although different reaction mechanisms can be envisaged for the three groups of ligands $\mathbf{L_1}$−$\mathbf{L_3}$, $\mathbf{L_4}$−$\mathbf{L_6}$, and $\mathbf{L_7}$, consistently with the significantly different E_p versus log v slopes and in accordance with the literature,[26] a rationalization of the $\mathbf{L_1}$−$\mathbf{L_6}$ reduction potentials can be obtained in terms of Hammett constants.[27] The linear correlation thus achieved (Figure 3) appears to be quite satisfactory, in spite

(25) Such normalized limiting current density only accounts for the number of globally transferred electrons and the diffusion coefficient of the reactant: $i_L/c = I_L/Ac = nFD^{1/2}$, where I_L = limiting current; i_L = limiting current density; A = electrode surface; c = substrate concentration in the bulk; n = number of transferred electrons; F = Faraday's constant = 96485 C mol^{-1} e^{-1}; D = diffusion coefficient of the reactant. See: Bard, A. J.; Faulkner, L. R. *Electrochemical Methods: Fundamentals and Applications*, 2nd ed.; Wiley: New York, 2001; pp 247–252.

Table 2. Selected CV Features for Ligands and Complexes Investigated in This Work (0.2 V s^{-1}, See Experimental Section)[a]

	first reduction peak				first oxidation peak				
ligands and complexes	$E_{p,cI}$[V]	$\lvert E_p - E_{p/2}\rvert$ [V]	$\lvert dE_p/d\log v\rvert$ [V]	$\lvert i_{L,\,conv}/c\rvert$ [A cm^{-2} mol^{-1} dm^3]	$E_{p,aI}$ [V]	$E_p - E_{p/2}$ [V]	$dE_p/d\log v$ [V]	$i_{L,conv}/c$ [A cm^{-2} mol^{-1} dm^3]	E_g [eV]
$\mathbf{L_1}$	–2.600	0.063	0.029	1.35					
$\mathbf{L_2}$	–2.638	0.067	0.029	1.17					
$\mathbf{L_3}$	–2.700	0.063	0.028	0.85					
$\mathbf{L_4}$	–2.318	0.070	0.053	0.68					
$\mathbf{L_5}$	–2.252	0.065	0.058	1.09					
$\mathbf{L_6}$	–1.992	0.058	0.040	0.91					
$\mathbf{L_7}$	–2.458	0.054	0.006	0.51					
1a	–1.345	0.057	0.002	0.48	1.315	0.037		0.76	2.66
1b	–1.365	0.056	0.002	0.32	1.163	0.030	0.006 → 0.035	0.66	2.53
1c	–1.378	0.073	0.001	0.29	0.944	0.037	0.002 → 0.032	0.62	2.32
2	–1.416	0.056	0.001	0.26	1.224	0.032	0.009 → 0.027	0.50	2.64
3	–1.457	0.058	0.004	0.32	1.271	0.030	0.006 → 0.022	0.57	2.73
4	–1.225	0.041	*b*	0.30	1.171	0.030	*b*	0.63	2.40
5	–1.252	0.057	0.001	0.32	1.176	0.032	0.005 → 0.038	0.70	2.43
6	–0.992	0.048	*b*	0.25	1.199	0.033	*b*	0.55	2.19
7	–1.532	0.040	0.023	0.34	1.244	0.030	0.010	0.61	2.78

[a] First cathodic and anodic peak potentials ($E_{p,cI}$ and $E_{p,aI}$), together with relevant half-peak widths ($E_p - E_{p/2}$), slopes of the linear E_p vs log v characteristics ($dE_p/d\log v$), normalized limiting currents after convolution ($i_{L,conv}/c$), and electrochemical energy gaps (E_g). Potentials are referred to the $Fc^+|Fc$ couple in the operating medium (MeCN + 0.1 M $TBAPF_6$). [b] Not determinable due to fast substrate solvolysis.

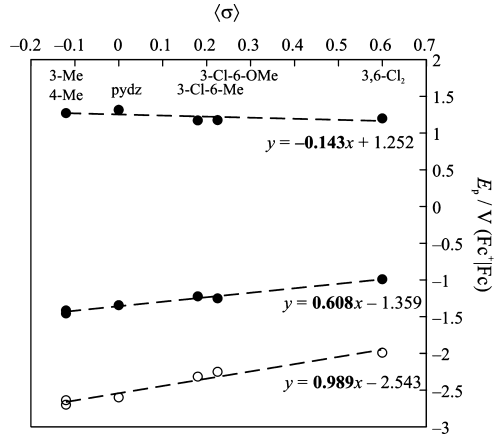

Figure 3. Correlations between peak potentials and averaged Hammett constants for pyridazine ring substituents. Empty symbols, $\mathbf{L}_n$ ligands; full symbols, complexes, for which two correlations are provided, accounting for the first oxidation peaks and the first reduction peaks.

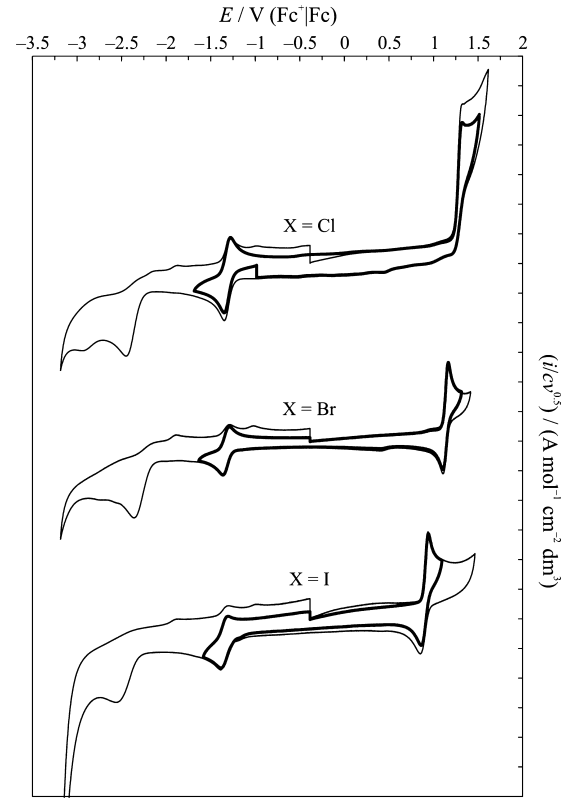

Figure 4. CV characteristics obtained for complexes **1a**, **1b**, and **1c**, at a 0.2 V s^{-1} scan rate, in MeCN, with 0.1 M $TBAPF_6$ as the supporting electrolyte, at 298 K, with ohmic drop compensation. Thin lines, complete CVs in the available potential window; thick lines, narrower CVs only including first oxidation and reduction peaks.

of the adoption of an averaged value of the meta and para σ parameters to account for substituents that are in the meta position with respect to one nitrogen atom and in the ortho or para position with respect to the other one.

Complexes. First Reduction Peak. The electrochemical activity of complexes **1–7** (Figures 4 and 5, Table 2) is remarkably different from those of the free ligands, even concerning the first reduction peaks, which are still ligand-centered (see below). In fact, such peaks are much more positive (1.0–1.2 V) for the complexes (**1a–6**) than for the corresponding ligands ($\mathbf{L_1}$–$\mathbf{L_6}$), implying that the coordination makes the ligand much electron-poorer. Moreover, the reduction is reversible, both from a chemical (symmetrical return peaks) and an electrochemical (facile electron transfer, accounted by the ≈57 mV half-peak widths and the nearly zero E_p versus log v slopes) point of view. In addition, it is monoelectronic, according to the i_L/c criterion, confirmed by the typical reversible peak morphological parameters.

This reduction is clearly ligand-centered, as demonstrated by the significant modulation of the peak potential by the diazine substituent (Figure 5) and by the negligible (although perceivable) effect of the halide ligand (Figures 4 and 6).

(26) (a) Lund, H. In *Organic Electrochemistry*, 4th ed.; Lund, H., Hammerich, O., Eds.; Dekker: New York, 2001; pp 695–696 andrefs therein. (b) Mubarak, M. S.; Peters, D. G. *J. Electroanal. Chem.* **2001**, *507*, 110–117. (c) Vieira, L. M. C.; Fonseca, A. M.; Raposo, M. M. M.; Kirsch, G. *Port. Electrochim. Acta* **2004**, *22*, 11–18.

(27) Hammett constants for aryl substituents in meta and para positions (σ_m and σ_p) and their average values $\langle\sigma\rangle$ are as follows: Me, −0.07, −0.17, −0.12; OMe, 0.12, −0.27, −0.08; Cl, 0.37, 0.23, 0.30: Zanello, P. *Inorganic Electrochemistry. Theory, Practice and Application*; The Royal Society of Chemistry: Cambridge, U.K., 2003; pp 572–582.

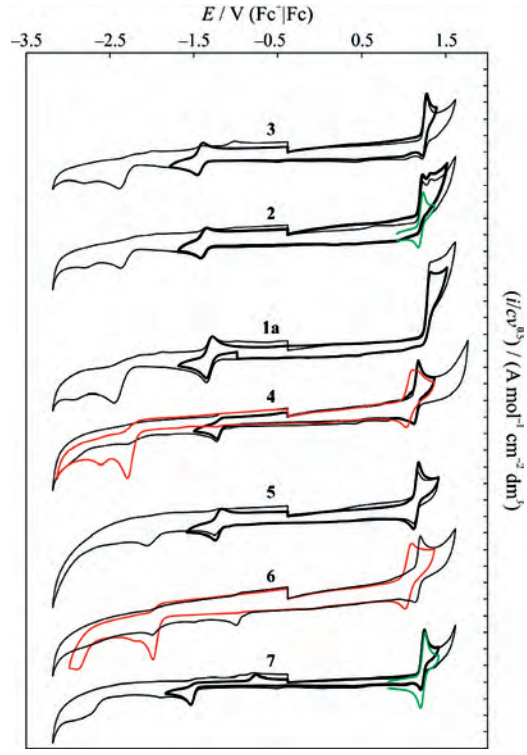

Figure 5. CV characteristics obtained for complexes **1a** and **2**–**7**, at a 0.2 V s^{-1} scan rate, in MeCN, with 0.1 M $TBAPF_6$ as the supporting electrolyte, at 298 K, with ohmic drop compensation. Thin lines, complete CVs in the available potential window; thick lines, narrower CVs only including first oxidation and reduction peaks; green lines, first oxidation peak at 2 V s^{-1}; red lines, same solution after complex solvolysis.

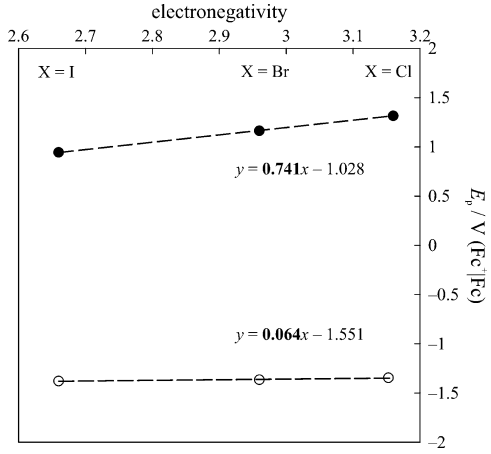

Figure 6. Correlations between first oxidation and reduction peak potentials and the electronegativity of the halide ligands, for complexes **1a**, **1b**, and **1c**.

The substituent effect on the reduction peaks is quite stronger for the ligand than for the complex (higher slope in Figure 3), in agreement with the nature of the LUMO of the complex, which is partially delocalized on the metal (see the Computational Study section).

The first reduction peak of the phthalazine derivative, **7**, shows a rather different behavior, because the return peak is displaced in the positive direction by many hundreds of millivolts. A chemical step following the electron transfer, resulting in the formation of an electrochemically active solid on the electrode surface, might explain this finding.

In all cases, the first reduction peak is followed by more complex peaks, whose interpretation, however, is beyond the aim of the present work.

Complexes. First Oxidation Peak. The oxidation is clearly metal-centered, as demonstrated by the poor modulation of peak potentials by the diazine substituents (Figure 3) and the strong modulation by the bridging halogen ligand. Figure 6 shows the fair linear correlation of E_{ox} with the halogen electronegativity (3.16, 2.96, and 2.66 for Cl, Br, and I, respectively), in agreement with the antibonding Re−halogen nature of the HOMO in these compounds (see below). The apparently anomalous behavior of the chlorinated pyridazine complexes, which exhibit lower oxidation potentials (i.e., easier oxidation) than **1a**, in spite of the electron-withdrawing character of the chloride group, can be explained by the destabilization of the HOMO upon substitution at the α positions (see below). The effect of the α substitution is also shown by the comparison between the peak potentials of **2** and **3**, the α-substituted ligand resulting in ≈50 mV peak anticipation.

The oxidation appears to be chemically reversible[28] and corresponds to a simultaneous two-electron transfer (the second electron is easier to give away than the first one; hence, it is lost concurrently with this one). This interpretation is supported by (a) the neat electrochemical reversibility or quasi-reversibility (nearly zero E_p versus log v slope, slightly increasing with increasing scan rate), (b) the neat ≈30 mV peak width, and (c) the neatly doubled i_L/c parameter with respect to the reduction one.

A simultaneous two-electron loss from a given site can be sometimes observed in polar solvents, where the solvation contribution (favorable to the creation of charged species, and higher than double in the case of a double-charged species with respect to a single-charged one) may prevail over the intrinsic major difficulty in removing an electron from a positively charged species.[29] Attempts to investigate the nature of the first oxidation process in a noncoordinating solvent such as CH_2Cl_2 failed because the oxidation peaks fell in close proximity of the background current.

The noninnocent nature of the working solvent (MeCN) is also demonstrated by the very fast solvolysis (eq 3, above) observed for complexes **4** and **6**, which contain particularly electron-poor ligands: in these cases, during the CV experiment, the solution rapidly faded and the bielectronic reversible oxidation peak changed into a monoelectronic reversible one (with a normalized peak current accounting for the oxidation of a substrate at double concentration). In the meanwhile, the first reduction peak of the complex disappeared, substituted by that of the free ligand (red curves in Figure 5). The positions of the oxidation peak[30] and of the ν(CO) bands[31] fully support the stoichiometry of eq 3. The

(28) Chemical reversibility appears impaired by fast following steps in the oxidations taking place at the highest potentials/energies, i.e., **1a**, and, to some extent, **2**, **3**, and **7**; although in these three latter cases, it is sufficient to increase the scan rate to neatly perceive the return peak (see Figure 5).

(29) Savéant, J.-M. *Elements of Molecular and Biomolecular Electrochemistry. An Electrochemical Approach to Electron Transfer Chemistry*; Wiley: New York, 2006; pp 62–74.

Table 3. Photophysical Data of the Complexes Described in This Work, in Toluene Solution at Room Temperature

compd	λ_{abs} ($\epsilon \times 10^{-3}$) [nm, M^{-1} cm^{-1}]	λ_{em}	$\Phi \times 10^2$	τ [ns]	$\eta_{isc}k_r \times 10^4$ [s^{-1}]	$k_{nr} \times 10^6$ [s^{-1}]
1a	379 (8.1)	600	5.2	715	7.3	1.3
1b	388 (6.8)	620	0.26	22	11.8	45.3
1c	394 (6.9)	(625)[a]	<0.01			
2	364 (7.0)	598	0.47	43	10.9	23.1
3	372 (8.8)	579	12.2	1250	9.7	0.70
4	375 (6.9)	(597)[a]	<0.01			
5	391 (7.9)					
6	400 (6.4)	(612)[a]	<0.01			
7	355 (8.6)	581	2.7	2260	1.2	0.43

[a] The emission of these compounds was very low and flat, so that the position of the maxima was affected by very high uncertainty and the measurement of lifetime and quantum yields was impossible.

anodic and cathodic peak currents were used to estimate the reaction rate (as shown in Figure S1 in the Supporting Information): $t_{1/2} = 6$ and 24 min, for **6** and **4**, respectively. In the case of **5**, fragmentation was much slower (ca. 20% after 1 h). For no other complex was decomposition observed in the time course of the electrochemical experiment.[32]

Finally, it is worthwhile to observe that in these complexes the oxidation appears more difficult (and the reduction easier) with respect to the classical mononuclear [$ReCl(CO)_3(N\text{-}N)$] complexes (about +0.3 V),[33] in agreement with the presence here of an electron-poorer $ReCl_2(CO)_3(N)$ core. The HOMO–LUMO gap is therefore similar in these two classes of complexes.

Photophysical Characterization. Absorption Spectra. The absorption spectra in CH_2Cl_2 solution of the three [$Re_2(\mu\text{-}X)_2(CO)_6(\mu\text{-pydz})$] complexes **1a**–**1c** show, in the higher energy region, bands attributable to transitions involving the carbonyl ligands or intraligand π–π^* transitions of the diazine. The latter were at 265–269 nm and little sensitive to the solvent, as in free pyridazine (250 nm).[34]

Moreover, all of the complexes show a broad low-energy absorption (355–400 nm), with molar absorbivity in the range 6400–8800 M^{-1} cm^{-1} (Table 3), that can be confidently assigned to a ^{1}MLCT transition by comparison with the tricarbonyl rhenium(I) complexes containing chelating diimine ligands. Typical of charge-transfer Re−L(π^*) absorptions are both the blue shift observed upon increasing the solvent polarity[35,36] (from 379 nm in toluene to 342 in MeCN for **1a**, Figure 7) and the red shift caused by the introduction of electron-withdrawing substituents on the diazine, which makes easier ligand reduction in the CT transition. Indeed, the absorption shifted from 364 nm for the complex with 3-Mepydz (**2**) to 400 nm for the complex with 3,6-Cl_2pydz (**6**, see Table 3).

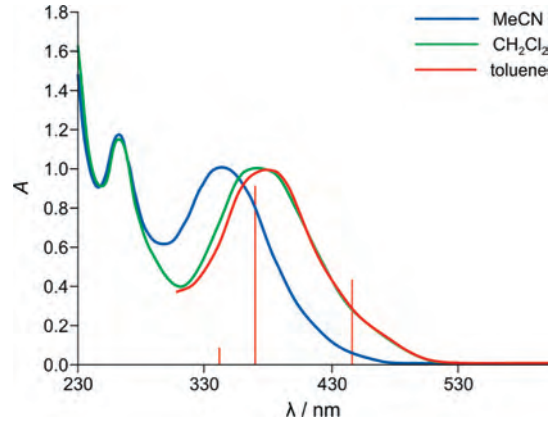

Figure 7. Solvent effect in the absorption spectra of [$Re_2(\mu\text{-Cl})_2(CO)_6(\mu\text{-pydz})$] (**1a**). A comparison with excitation energies and oscillator strengths (vertical red lines) computed in toluene is reported.

As expected for a MLCT transition, the absorption maxima shift to lower energy upon changing the halide ligands from Cl to Br to I, because the oxidation of the metal becomes progressively easier upon decreasing the electronegativity of the halide. This trend is parallel to that of the electrochemical energy gaps (E_g) of Table 2.

The effects of the substitution on the diazine ring have been checked in the series of the dichloro derivatives [$Re_2(\mu\text{-Cl})_2(CO)_6(\mu\text{-diaz})$] (Table 3). The presence of a Me group (**2** and **3**) or of a fused aromatic ring (**7**) induces a blue shift in the absorption spectra, while the opposite occurs for the chlorinated derivatives (**5** and **6**). This trend roughly corresponds to the variation of the electrochemical E_g, but the correlation is rather poor ($R^2 = 0.71$, Figure 8). The lack of correlation is particularly clear for the 3-Cl−6-Me derivative, **4**, which shows a (slight) blue shift with respect to **1a** (375 vs 379 nm), in spite of its smaller E_g (2.40 vs 2.66 eV). This might imply that the electronic transitions responsible for the observed absorption bands do not have a strict HOMO–LUMO character, as confirmed by the computations reported below.

Photoluminescence Spectra. Most of the new complexes are photoluminescent in solution at room temperature. Upon excitation in the range 300–454 nm, broad unstructured emission is observed at wavelengths in the range 579–620 nm, that is, in the same spectral region of the other known diimine tricarbonyl species. It has been checked that emission is independent of the excitation wavelengths and that the complexes are photostable.

(30) Brisdon, B. J.; Edwards, D. A.; Towell, I. M.; Moehring, G. A.; Walton, R. A. *J. Chem. Soc., Dalton Trans.* **1988**, 245–247.
(31) Farona, M. F.; Kraus, K. F. *Inorg. Chem.* **1970**, *9*, 1700–1704.
(32) ^{1}H NMR monitoring revealed a different and much slower ($t_{1/2} > 2$ days) decomposition pathway for the prototypical complex **1a** in CD_3CN solution. In this case, the NMR data showed that pyridazine remained coordinated, passing from a bridging to a terminal position, affording most likely [$Re_2(\mu\text{-Cl})_2(CO)_6(diaz)(MeCN)$].
(33) Richter, M. M.; Debad, J. D.; Striplin, D. R.; Crosby, G. A.; Bard, A. J. *Anal. Chem.* **1996**, *68*, 4370–4376, and refs therein.
(34) Halverson, F.; Hirt, R. C. *J. Chem. Phys.* **1951**, *19*, 711–718.
(35) Drago, R. S. *Physical Methods in Chemistry*; W. B. Saunders Company Ed.: Philadelphia, PA, 1977.
(36) See also: Giordano, P. J.; Wrighton, M. S. *J. Am. Chem. Soc.* **1979**, *101*, 2888–2897, and refs therein.

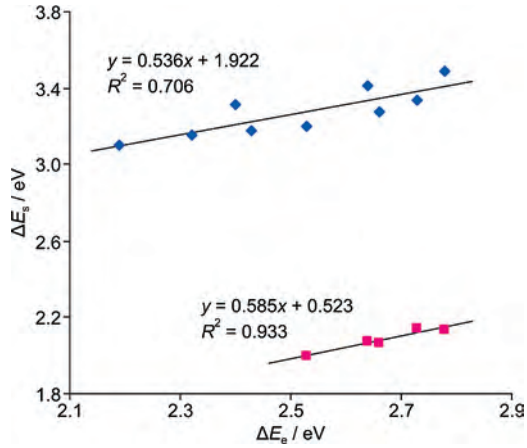

Figure 8. Correlation between the spectroscopic (absorption, blue diamonds; emission, purple squares) and the electrochemical energy gaps (E_g in Table 2).

Table 4. Solvent Effect on the Photophysical Properties of Compound **1a**

solvent	λ_{abs} ($\epsilon \times 10^{-3}$) [nm, M^{-1} cm^{-1}]	λ_{em}	$\Phi \times 10^2$	τ [ns]
toluene	379 (8.1)	600	5.2	715
CH_2Cl_2	375 (7.9)	613	4.4	430
MeCN	342 (7.9)	626	1.8	367

Table 3 collects the photophysical data for the complexes in toluene solution, while Table 4 shows the effect of the medium on the properties of the prototypical compound **1a**. The emission maximum is solvent-dependent (from 600 nm in toluene to 626 nm in acetonitrile for **1a**), as is characteristic of ^{3}MLCT emission.[37–39] The blue shift of the emission in the less-polar solvents (opposite with respect to that observed in the absorption) is accompanied by an increase of its intensity and of its lifetime (see Table 3), in agreement with the energy gap law (EGL).[40]

Upon varying the halide ligand (in the series **1a**–**1c**), a slight red shift of the emission maxima is observed, even smaller than that of the corresponding absorptions (from 2.07 to ≈1.98 eV, although the very low emitting properties of **1c** did not allow evaluation with accuracy of the latter value). The parallel strong drop of the quantum yields (Figure 9a), as well as the decrease of lifetime on going from Cl to Br, are qualitatively in line with the EGL requirements but too large to be explained by the small energy gap decrease only. This trend is opposite to that seen in mononuclear [ReX(CO)$_3$(bpy)] complexes,[9b] where both τ and Φ significantly increased from Cl to I, without a significant decrease of the emission energy.[41] In our case, it is possible that the progressive increase of halogen size imposes severe distortions to the coordination sphere, making it less rigid and therefore more keen to vibrationally induced de-excitation pathways. This point will be further discussed in the computational part of the work.

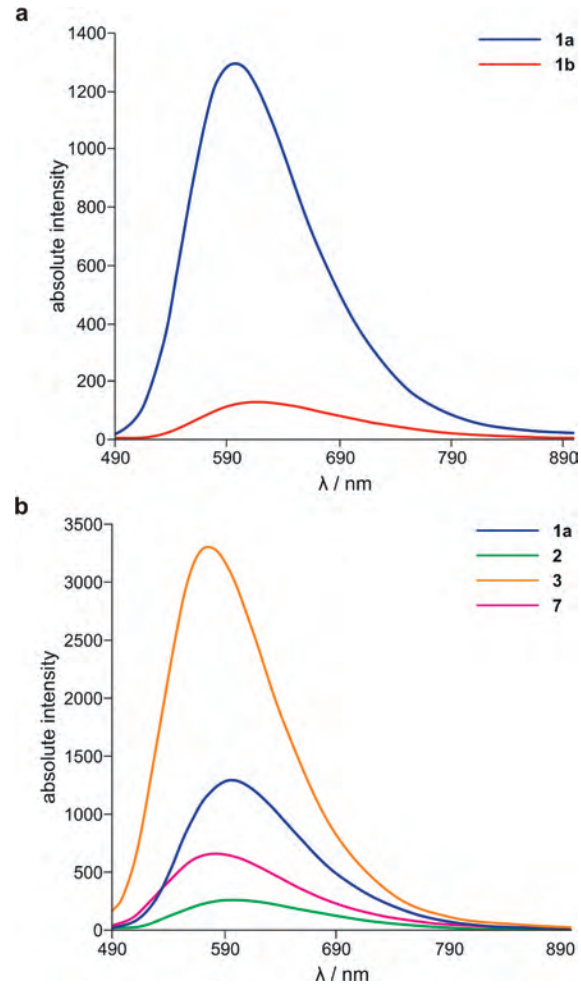

Figure 9. (a) Effect of the halogen substitution on the emission spectrum of [$Re_2(\mu$-X)$_2$(CO)$_6$(μ-pydz)] (toluene solution). (b) Effect of the substitution of the diazine on the emission spectrum of [$Re_2(\mu$-Cl)$_2$(CO)$_6$(μ-diaz)] (toluene solution).

As to the effects of the variation of the substituents on the diazine (Table 3), the same species that show a blue shift in the absorption (**2**, **3**, and **7**) exhibit a blue shift also in the emission spectra (although this effect is almost negligible in the emission of **2**). The correlation with the electrochemical ΔE is much better than that of the absorption data (R^2 = 0.93, Figure 8).

The complexes showing the highest emission quantum yields (**1a**, **3**, and **7**, Table 3) have also the longest lifetimes (on the order of microseconds, which is a further proof of emission arising from a prevalently ^{3}MLCT state). The values of Φ/τ (= $k_r\eta_{isc}$, where the latter term represents the efficiency of the intersystem crossing process) are in the range (1–11) $\times$ 10^4 s^{-1} for all of the emitting species (see Table 3), as is usually observed for related emitters. The short lifetime and the low quantum yields of the 3-Mepydz derivative can be attributed to the steric crowding arising from the α substitution of the diazine ring, which causes a lengthening of the metal−diazine distance, making

(37) (a) Shaw, J. R.; Schmehl, R. H. *J. Am. Chem. Soc.* **1991**, *113*, 389–394. (b) Wallace, L.; Rillema, D. P. *Inorg. Chem.* **1993**, *32*, 3836–3843.
(38) Valeur, B. *Molecular Fluorescence. Principles and Applications*; Wiley-VCH: Weinheim, Germany, 2002.
(39) Baba, H.; Goodman, L.; Valenti, P. C. *J. Am. Chem. Soc.* **1966**, *88*, 5410–5415.
(40) Lacowicz, J. R. *Principles of Fluorescence Spectroscopy*, 2nd ed.; Kluwer: New York, 1999.
(41) This was attributed to a change of the nature of the lowest-excited state from MLCT to interligands XLCT transitions on changing the halogen: Rossenaar, B. D.; Stufkens, D. J., Jr *Inorg. Chem.* **1996**, *35*, 2902–2909.

Table 5. Optimized Geometrical Parameters [pm, deg] for the Ground-State of the Complexes $[Re_2(\mu\text{-}X)_2(CO)_6(\mu\text{-diaz})]$[a]

	μ-diaz	μ-X	Re···Re	Re−X	Re−N	N−N	X−Re−X	Re−N−N	Re···Re−C(axial)
1a	pydz	Cl	355.8	252.1	221.7	133.1	81.72	120.15	114.80
1b	pydz	Br	363.1	265.2	222.5	133.1	83.68	121.13	116.17
1c	pydz	I	373.3	284.3	223.4	133.3	86.00	122.50	117.95
	3,6-Me_2pydz	Cl	352.0	251.1	230.1	135.0	85.14	118.13	109.86
	4,5-Me_2pydz	Cl	356.3	252.2	222.0	132.7	81.64	120.25	114.84
6	3,6-Cl_2pydz	Cl	353.2	251.2	229.6	135.5	84.60	118.30	110.52
	4,5-Cl_2pydz	Cl	356.1	252.1	221.9	133.2	81.66	120.15	114.75
2	3-Mepydz	Cl	354.3	251.9 251.4	227.9 223.5	133.8	83.07 83.26	115.97 122.57	111.04 114.42
3	4-Mepydz	Cl	356.0	252.2 252.2	222.1 221.8	132.9	81.79 81.78	119.99 120.36	114.72 114.83
4	3-Cl-6-Mepydz	Cl	352.6	251.3 251.0	230.2 229.7	135.3	84.84 84.99	118.88 117.52	109.82 110.45
5	3-Cl-6-OMepydz	Cl	354.0	251.6 251.6	228.6 226.5	134.4	83.95 83.94	117.30 120.40	110.97 112.04

[a] For the C_s symmetric species, two values for some of the parameters are reported.

less stiff the structure of the diazine−$Re_2(\mu\text{-}Cl)_2$ chromophore (see the Computational Study section).

The quantum yields found for these dinuclear diazine complexes are slightly higher than those of the classical $[ReX(CO)_3(N{-}N)]$ mononuclear complexes containing chelating diimines: compare for instance the value measured for **1a** in CH_2Cl_2 (0.044) with the values reported for the prototypical $[ReCl(CO)_3(bpy)]$ and $[ReCl(CO)_3(phen)]$ species in the same solvent (0.005[11a] and 0.036,[1] respectively).

Computational Study. Some pyridazine rhenium complexes were studied by means of density functional and time-dependent density functional (TD-DFT) calculations. Computational details can be found in the Experimental Section. All of the synthesized pyridazine complexes (**1**–**6**) were investigated, along with the derivatives of some other symmetrical ligands (3,6-Me_2pydz, 4,5-Me_2pydz, and 4,5-Cl_2pydz). As a consequence, steric and electronic effects associated with the introduction of electron-withdrawing and -donating substituents at the α and β positions of the pyridazine ring could be evaluated and compared. In addition, the effect of changing the nature of the bridging halogen ligands was also examined.

Ground-State Optimized Geometry and Relative Stability. All of the complexes possess the highest possible symmetry (C_{2v} and C_s for symmetrically and asymmetrically substituted pyridazines, respectively). The most relevant geometrical parameters are reported in Table 5 (for a complete list, see Table S2 in the Supporting Information). Ground-state optimized geometry for **1a** well compares to the X-ray experimental structure.[42]

The effect of the bridging-halogen size can be recognized by comparing the geometry of the three unsubstituted pyridazine complexes **1a** (Cl), **1b** (Br), and **1c** (I). The increase in the covalent radius on going from Cl to Br to I leads to a noticeable change in geometrical parameters involving the μ-X ligand, in particular, the Re−X bond distance. As a consequence, the Re···Re distance increases as well, leading to a poorer overlap between the metal atoms and the nitrogen lone pairs of the bridging pyridazine ligand (an optimal coordination geometry requires a Re···Re distance of 323 pm[43]). To partially overcome this problem, the rhenium-centered coordination octahedra bend toward the nitrogen atoms (as can be deduced by the widening of the Re···Re−C(axial) angle), leading to unfavorable steric interactions between the equatorial carbonyl ligands and the diazine. It is possible to conclude that the larger the halogen, the weaker is the interaction between the pyridazine and the metal dimer.

Pyridazine substitution at a β position leads to only minor geometrical changes. On the contrary, substitution at the α positions leads to a marked lengthening of the Re−N bond and a noticeable bending of the rhenium-centered octahedra (see the shrinking of the Re···Re−C(axial) angle in Table 5) as a consequence of the repulsion between the diazine and the equatorial carbonyl ligands. This effect can be especially appreciated by comparing "equivalent" bond distances and angles of the asymmetrically substituted 3-Mepydz derivative **2**.

However, the strength of the diazine binding to the metal core is affected not only by steric hindrance but also by the donor capability of the aromatic ligand. Indeed, the interaction energy[44] computed for all of the diazine complexes (that is, the energy difference between the complex and the separated ligand and metal moieties, see Experimental Section) well correlates with a combination of the steric and electronic descriptors reported in Table 1. Ligand repulsive energy (a molecular-mechanics-derived parameter introduced by Brown[45]) was chosen as a measure of steric effects, while charge transfer between the diazine and the $Re_2(\mu\text{-}X)_2(CO)_6$ fragment (derived from a natural population analysis[46]) was chosen as a measure of electronic effects. Relative repulsive energy values can be easily interpreted in terms of the position, the number, and the volume (Me > Cl ≈ OMe > H) of the diazine substituents. Charge transfer depends on

(42) Mean and maximum absolute deviations in bond distances (1.6 and 2.3 pm) and bond angles (0.9 and 2.8°) are small, particularly if the standard deviations of the experimental data are taken into account. See Table S3 in the Supporting Information.

(43) Computed from the mean M–N–N bond angle (115.3°), the mean N−N bond distance (135 pm), and the mean Re−N bond distance (220 pm) of nonbridging pyridazine-κ*N* complexes. Data were retrieved from the Cambridge Structural Database, CSD version 5.28 (November 2006): Allen, F. H. *Acta Crystallogr., Sect. B: Struct. Sci.* **2002**, *58*, 380–388.

(44) Zhang, J.; Frenking, G. *Chem. Phys. Lett.* **2004**, *394*, 120–125.

(45) (a) White, D. P. In *Computational Organometallic Chemistry*; Cundari, T. R., Ed.; Dekker: New York, 2001; pp 39–67. (b) Brown, T. L. *Inorg. Chem.* **1992**, *31*, 1286–1294.

(46) Weinhold, F.; Landis, C. R. *Valency and Bonding. A Natural Bond Orbital Donor-Acceptor Perspective*; Cambridge University Press: Cambridge, U.K., 2005.

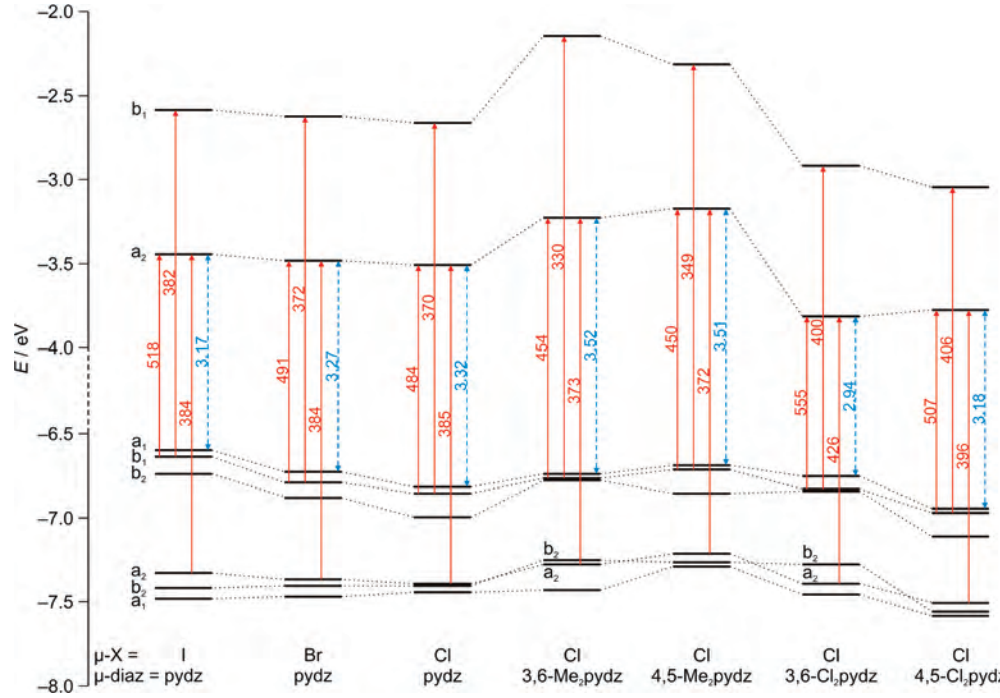

Figure 10. Partial molecular orbital diagrams for the C_{2v}-symmetric diazine complexes $[Re_2(\mu\text{-}X)_2(CO)_6(\mu\text{-diaz})]$ (X = Cl, Br, and I; diaz = pydz, 3,6-Me_2pydz, 4,5-Me_2pydz, 3,6-Cl_2pydz, and 4,5-Cl_2pydz). Red arrows correspond to absorption electronic transitions (gas-phase TD-DFT wavelength values [nm] are given). Blue dashed arrows highlight HOMO–LUMO gaps (DFT energy values [eV] are given).

the nature and the number of substituents, whose donation power follows the order Me > H > Cl ≈ OMe.

In conclusion, both substitution at the α position and the presence of electron-withdrawing groups have detrimental effects on the stability of the diazine complex, leading to the following sequence for the overall interaction energy: 4,5-Me_2pydz > 4-Mepydz > pydz > 3-Mepydz > 3,6-Me_2pydz > 4,5-Cl_2pydz > 3-Cl-6-OMepydz > 3-Cl-6-Mepydz > 3,6-Cl_2pydz. The low stability of the latter two species was proved by their fast decomposition in acetonitrile solution during the CV measurements (see above).

As far as changes in bridging halogens are concerned, the already described steric effects, together with the electronegativity changes, leads to the following sequence for the overall interaction energy: **1a** (Cl) > **1b** (Br) > **1c** (I).

Electronic Structure. Partial molecular orbital diagrams for the C_{2v}-symmetric diazine complexes under study are reported in Figure 10, while isodensity surface plots of some relevant molecular orbitals for the unsubstituted compound **1a** are depicted in Figure 11. In the following, mainly the C_{2v}-symmetric complexes will be discussed. However, analogous considerations can be drawn for the C_s-symmetric species, taking into account the appropriate changes in symmetry labels.[47]

The six HOMOs correspond to the "t_{2g}" set of the two rhenium atoms in a pseudo-octahedral environment. The three lowest levels (from HOMO − 5 to HOMO − 3) are essentially nonbonding combinations of rhenium d orbitals

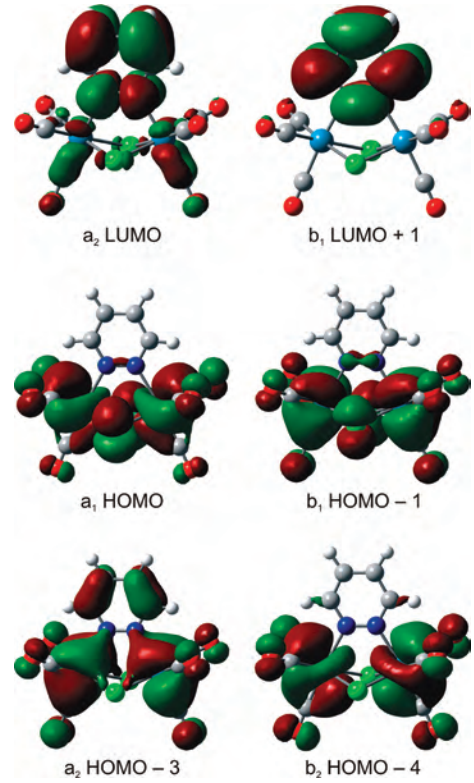

Figure 11. Isodensity surface plots of some relevant molecular orbitals of $[Re_2(\mu\text{-}Cl)_2(CO)_6(\mu\text{-pydz})]$ (**1a**).

with minor contributions from the ligands (mainly carbonyl π^* orbitals). In addition, in the a_2 orbital, a significant contribution from the pyridazine LUMO can be recognized. The three remaining HOMOs are Re-(μ-X) π^* orbitals, once again with small contributions from the carbonyl π^* orbitals.

(47) Symmetry labels change as follows: A_1 and B_2 become A' while A_2 and B_1 become A'' (choosing σ_h orthogonal to the x axis). Altmann, S. L.; Herzig, P. *Point-Group Theory Tables*; Oxford University Press: Oxford, U.K., 1994.

The two LUMOs are essentially the two lowest-lying π^* orbitals of the diazine (the remaining all-antibonding combination of p orbitals is much higher in energy).

Bridging halogen ligands mainly contribute to the three highest occupied molecular orbitals. As a consequence, only these levels are significantly affected by changes in the nature of the halogen, and the trend in the HOMO energy for **1a**–**1c** follows the decrease in electronegativity down the group (Figure 10). On the contrary, the LUMO energy of the three species is similar. The HOMO–LUMO gap, therefore, decreases upon going from the chlorine to the iodine derivative.

Substitution at the α and β positions of the pyridazine ring is more complex to analyze, since different factors contribute toward the observed trend. The more affected orbitals are the two LUMOs whose behavior parallels that of the corresponding free diazine: as expected, electron-donating groups destabilize these orbitals, while electron-withdrawing groups stabilize them.[48] The effect of substitution is, however, somehow reduced in the diazine complexes with respect to the free ligands, due to the metal contribution to the LUMO of the complexes.

The diazine LUMO directly contributes to the a_2 nonbonding highest occupied orbital as well. As a consequence, changes in the LUMO energy upon substitution are mirrored by (smaller) changes in the energy of the highest occupied a_2 orbital. To an even more limited extent, a similar trend can also be observed for the other HOMOs.

However, the behavior of some of the HOMOs seems to be more related to the geometrical changes dictated by the presence of substituents on the diazine ring than to their electronic properties. In particular, the HOMO ordering in the α-substituted complexes differs from that of the remaining species, since substitution at the α position causes major distortions of the $Re_2(\mu\text{-}Cl)_2$ core, and therefore affects the energy of the HOMOs, which are mainly Re−Cl antibonding or Re···Re nonbonding in character. In particular, the metal−core contraction destabilizes the two highest occupied b_2 orbitals (Figure 11), since they contain out-of-phase (nonbonding) combinations of rhenium d orbitals.

In summary, the trend in HOMO–LUMO gaps upon substitution can be interpreted in terms of the electron-withdrawing and -donating properties of the substituents. The geometrical distortions determined by substitution at the α position can however modify this simplified picture.

Electronic Transitions Involved in the Absorption Spectra. In order to simulate the absorption electronic spectrum of the diazine complexes down to 300 nm, the lowest 20 singlet excitation energies were computed. However, for most of the transitions, the oscillator strength *f* is negligible, and only the three singlet excitations for which $f > 0.01$ are depicted in Figure 10, and the most intense one is reported in Table 1.[49]

The starting orbital involved in the two less-intense transitions ($f = 0.01$–0.07) is the highest occupied b_1 orbital (HOMO – 1), while the final orbitals are the LUMO (a_2) and LUMO + 1 (b_1). The more intense transition ($f = 0.10$–0.19) involves as the starting orbital the highest occupied a_2 orbital (HOMO – 3 or, for species substituted at the α position, HOMO – 4) and as the final orbital the LUMO.

Due to the presence of significant contribution from the ligands to the metal-centered starting orbitals, these transitions are better described as metal–ligand-to-ligand charge transfers. The computed wavelengths are in fair agreement with the experimental absorption maxima measured in toluene solution. Mean and maximum absolute deviation between the experimental λ_{max} and the wavelength for the more intense $a_2 \rightarrow a_2$ transition computed in the gas phase are 14 and 26 nm, respectively. The agreement slightly improves (the mean and maximum absolute deviation reduce to 9 and 23 nm, respectively), including the toluene solvent in the calculation, employing the conductor-like polarizable continuum model (CPCM). In Figure 7, the low-energy portion of the experimental absorption spectrum of **1a** is compared to the excitation energies and oscillator strengths computed in toluene.

As far as the emissive behavior of these species is concerned, an important property is the transition probability, proportional to the intensity of the emitted radiation. This quantity, as long as spin–orbit coupling is not explicitly taken into account, cannot be computed since the $T_1 \rightarrow S_0$ transitions are spin-forbidden, leading to a nil value of the oscillator strength. However, since the amount of the metal atom contribution to the orbitals involved in the emission process is similar along the series of compounds under study, the radiative rate constants should be almost identical for all of these species, as indeed oberved (see Table 3). Differences in the measured quantum yields can be therefore tentatively attributed to the extent of nonradiative de-excitation. It is interesting to note that molecules showing sizable quantum yields show indeed high values of the interaction energy between the diazine ligand and the $Re_2(\mu\text{-}X)_2$ core, hence, stiffer metal–ligand bonds.

Conclusion

The present work reports the first detailed investigation on the luminescence properties of a new class of transition metal complexes containing 1,2-diazine ligands. Despite the lability of these ligands in coordinating solvents such as acetonitrile, the dinuclear $[Re_2(\mu\text{-}X)_2(CO)_6(\mu\text{-diaz})]$ complexes have revealed photophysical properties comparable to those of the classical $[ReX(CO)_3(N\text{-}N)]$ mononuclear complexes: ligand-centered reduction (in LUMOs that are mainly ligand-π^* orbitals), metal-centered oxidation (although the HOMOs here are antibonding Re−halogen−Re

(48) A list of HOMO and LUMO energies for both the diazine ligands and the corresponding rhenium complexes can be found in Table S4 (Supporting Information).

(49) A list of the three more-intense singlet excitations can be found in Table S5 (Supporting Information). TD-DFT describes excited states as linear combinations of singly excited configurations. Transitions reported in Table S6 can be described by using the three one-electron excitations between pairs of ground-state orbitals depicted in Figure 10. These three excitations account for more than 90% of the transitions discussed. No other one-electron excitation between pairs of ground-state orbitals is significantly involved.

orbitals and the oxidation is bielectronic), a similar HOMO–LUMO gap (ca. 2.7 eV, with both HOMO and LUMO more stable by about 0.3 eV with respect to the mononuclear species), emission at wavelengths close to 600 nm, and lifetimes up to thousands of nanseconds. Even from the point of view of the emission efficiency, the properties of these complexes in nonpolar solvents have been found to be comparable, if not superior, to those of the classical $[ReX(CO)_3(N\text{-}N)]$ mononuclear complexes. In fact, the quantum yield found for compound **3** ($\Phi = 0.122$) represents, to the best of our knowledge, the highest value ever reported for a *neutral* $Re(CO)_3$ complex.

It appears therefore worthwhile to continue the studies on this new class of complexes. It is well-known that even little changes of the ancillary ligands or of the substituents on the heterocycle can dramatically modify the photophysics of the emitting complexes: in the present case, the nature of the bridging ligand X and of the substituents on the diazine have a major effect on the emission quantum yields (while affecting in a minor way the energy of the emitted radiation). With respect to the mononuclear $[ReX(CO)_3(N\text{-}N)]$ species, the presence here of two bridging ancillary ligands enables a richer possibility of modulation of the ligands sphere. The computational studies here reported give useful indications on the ways to follow.

In particular, these studies have clarified the nature of the orbitals involved in the electronic transitions and described the steric and electronic consequences of pyridazine substitution on the geometry of these species. Moreover, they have shown that an easily determinable parameter such as the interaction energy provides faithful information on the stiffness of the metal–ligand bond and therefore on the easiness of radiationless de-excitation processes. This in turn well correlates with the quantum yields of emission, since, in a homologue series of complexes like those here reported, radiative rate constants are expected to be similar. For many applications, quantum yield is the most important photophysical property, but unfortunately it is the Achilles' heel of even sophisticated state-of-the-art theoretical computations. The interaction energy might therefore provide in many cases this precious missing predictive parameter on the emission efficiency.

On this ground, future work aimed at the synthesis of stable complexes with high emitting power will point to an increase in the interaction energy and to satisfying the geometrical requirements of the bridging coordination. Therefore, 1,2-diazine made electron-richer by suitable substitution at the β positions will be employed, as well as $Re_2(\mu\text{-}X)_2$ cores containing bridging groups with small and electronegative donor atoms.

Experimental Section

All reactions were performed under N_2 using the Schlenk technique. All of the solvents were deoxygenated and dried by standard methods. Pyridazine (pydz), phthalazine, 3,6-Cl_2pydz (Aldrich), 3-Cl-6-Mepydz, 3-Cl-6-OMepydz, 3-Mepydz, and 4-Mepydz (Lancaster) were used as received. $[ReX(CO)_5]$ and $[Re_2(\mu\text{-}X)_2(CO)_8]$ were prepared according to literature procedures.[50,51] ^1H NMR spectra were recorded on Bruker DRX300 or DRX400 spectrometers. IR spectra were acquired on a Bruker Vector 22 FT instrument. Electronic absorption spectra were recorded on a Jasco V-570 spectrophotometer, at room temperature.

Synthesis of the $[Re_2(\mu\text{-}X)_2(CO)_6(\mu\text{-diaz})]$ derivatives 1–7. The complexes were prepared as follows: 50 mg of $[ReX(CO)_5]$ was dissolved, upon heating, in 20 mL of freshly distilled toluene, in a Schlenk tube; then, 0.5 equiv of 1,2-diazine was added. The solution was refluxed for 1 h, then evaporated to dryness under a vacuum to give a yellow to red residue. Dissolution in CH_2Cl_2 and precipitation with *n*-hexane afforded microcrystalline samples (isolated yields 60–80%). The preparation from $[Re_2(\mu\text{-}X)_2(CO)_8]$ was performed in the same way, on using 1 equiv of the diazine. Table S1 (Supporting Information) summarizes the spectroscopic and analytical data of the products. For photophysical measurements and for the X-ray characterization of **1a**, the products were crystallized by diffusion of *n*-hexane into CH_2Cl_2 solutions at 248 K.

Electrochemical Measurements. The cyclovoltammetric study of the complexes and of the corresponding $\mathbf{L_n}$ ligands has been performed at scan rates typically ranging from 0.02 to 10 V s^{-1}, in HPLC-grade acetonitrile solutions at 0.000 25–0.001 M concentration in each substrate, deareated by N_2 bubbling, with 0.1 M tetrabutylammonium hexafluorophosphate ($TBAPF_6$; Fluka) as the supporting electrolyte, at 298 K. The ohmic drop has been compensated by the positive feedback technique.[52] The experiments were carried out using an AUTOLAB PGSTAT potentiostat (EcoChemie, The Netherlands) run by a PC with GPES software. The working electrode was a glassy carbon one (AMEL, diameter = 1.5 mm) cleaned by diamond powder (Aldrich, diameter = 1 μm) on a wet cloth (STRUERS DP-NAP); the counter electrode was a platinum wire; the reference electrode was an aqueous saturated calomel electrode, having in our working medium a difference of −0.385 V versus the $Fc^+|Fc$ couple (the intersolvental redox potential reference currently recommended by IUPAC)[53] and +0.032 V versus the $Me_{10}Fc^+|Me_{10}Fc$ couple (an improved intersolvental reference under investigation).[54]

Photophysical Measurements. Steady-state fluorescence measurements have been performed with a calibrated optical multichannel analyzer (Hamamatsu PMA-11), at room temperature. The solutions were prepared under N_2 by introducing the quartz cuvettes into a suitable Schlenk tube and were deoxygenated by bubbling Ar during measurements. Sample fluorescence has been excited by a CW diode laser at 407 nm (15 mW power), and the signal has been collected through a 420-nm-long pass filter to avoid scattering contributions to the spectra. The emission intensities have been normalized to a nominal absorption value of 0.1. Quantum yields have been determined by comparison with the emission of $[Ru(bpy)_3]Cl_2$ in acetonitrile ($\Phi = 0.062$).[55]

(50) Schmidt, S. P.; Trogler, W. C.; Basolo, F. *Inorg. Synth.* **1985**, *23*, 41–46.
(51) Abel, E. W.; Hargreaves, G. B.; Wilkinson, G. *J. Chem. Soc.* **1958**, 3149–3152.
(52) Bard, A. J.; Faulkner, L. R. *Electrochemical Methods. Fundamentals and Applications*; Wiley: New York, 2002; pp 648–650.
(53) (a) Gritzner, G.; Kuta, J. *Pure Appl. Chem.* **1984**, *56*, 461–466. (b) Gritzner, G. *Pure Appl. Chem.* **1990**, *62*, 1839–1858.
(54) (a) Noviandri, I.; Brown, K. N.; Fleming, D. S.; Gulyas, P. T.; Lay, P. A.; Masters, A. F.; Phillips, L. *J. Phys. Chem. B* **1999**, *103*, 6713–6722. (b) Ruiz, J.; Astruc, D. *C. R. Acad. Sci., Ser. IIc: Chim.* **1998**, *I*, 21–27. (c) Falciola, L.; Gennaro, A.; Isse, A. A.; Mussini, P. R.; Rossi, M. *J. Electroanal. Chem.* **2006**, *593*, 47–56.
(55) Caspar, J. V.; Meyer, T. J. *J. Am. Chem. Soc.* **1983**, *105*, 5583–5590.

Dynamic fluorescence measurements have been performed with a frequency modulated phase fluorometer (Digital K2, I.S.S., Urbana, IL). The excitation was accomplished by the 30 mW output of the 454.5 nm line of an argon ion laser (2025, Spectra Physics, Mountain View, CA). At least 15 data points at logarithmically spaced frequencies in the range 0.3–60 MHz with a cross-correlation frequency of 80 Hz have been acquired for lifetime measurements. The convenient accuracy for phase angles and modulation ratios has been 0.2° and 0.004, respectively. Lifetime measurements have been performed under the magic angle conditions, and a 535-nm-long pass filter (Andover Co.) has been employed in order to cut light scattering. A solution of glycogen in doubly distilled water has been used as the reference sample.[56] Lifetime data fitting has been accomplished by an ISS routine based on the Marquardt least-squares minimization, with a two-exponential decay scheme in order to take into account the scattering contribution to the overall signal. The fit of the fluorescence intensity decay $F(t)$ yields the lifetime values τ_i together with the corresponding fractional intensities f_i: $F(t) = \sum \alpha_i e^{-t/\tau_i}$ and $f_i = \alpha_i\tau_i/\sum\alpha_i\tau_i$, where α_i represent the pre-exponential factors.

The photostability of the different samples has been assessed indirectly by verifying that the fluorescence emission at the beginning and end of the lifetime measurement session did not change with respect to the reference (glycogen) emission. Since at least two lifetimes have been recorded for each sample, no variation in the sample fluorescence intensity has been observed on a time scale of about 60 min.

Computational Details. Ground-state geometries were optimized by means of density functional calculations. The parameter-free hybrid functional PBE0[57] was employed along with the standard valence double-ζ polarized basis set 6-31G(d,p) for C, H, Cl, N, and O. For Re, Br, and I, the Stuttgart-Dresden effective core potentials were employed along with the corresponding valence triple-ζ basis set and a set of polarization functions on Br and I ($\alpha_{d,Br} = 0.389$, $\alpha_{d,I} = 0.266$). To check the effect of basis set expansion, explorative calculations employing the 6-311++G(2d,2p) basis set were done on **1a**, obtaining negligibly different results (max change in bond distances and angles:, 0.8 pm and 1.3°; max change in computed energy differences, 0.08 eV; max change in computed wavelengths, 9 nm).

All of the calculations were done assuming C_{2v} or C_s symmetry. The nature of all of the stationary points was checked by computing vibrational frequencies, and all of the species were found to be true minima.

Instantaneous interaction energy was computed as the absolute value of the (counterpoise-corrected[58]) energy difference between the complex and the separated ligand and metal moieties computed using the frozen geometry of the complex.[44]

Ligand repulsive energy[46] is defined by $E_r = -r_0(\partial E_{vdW,r}/\partial r)$, in which r_0 is the equilibrium metal–ligand distance and $E_{vdW,r}$ is the repulsive component of the van der Waals potential. When the bridging diazine ligands are dealt with, the metal–ligand vector was defined by means of the midpoints of the N−N and Re−Re dumbbells. Standard UFF van der Waals functional form and parameters were used.[59]

In order to simulate the absorption electronic spectrum down to 300 nm, the lowest 20 singlet excitation energies were computed by means of time-dependent density functional calculations. Calculations were done also in the presence of solvent (toluene, used in most of the photophysical characterizations) described by CPCM.[60]

All of the calculations were done with Gaussian 03.[61]

Acknowledgment. We thank Italy's MIUR for financial support (FIRB 2003, RBNE033KMA, Molecular compounds and hybrid nanostructured material with resonant and non-resonant optical properties for photonic devices). The authors are indebted to Dr. M. Muccini and Dr. S. Toffanin (CNR-ISMN Bologna) for the steady-state photoluminescence measurements.

Supporting Information Available: Analytical and spectroscopic data for **1–7**, optimized geometries and computed electronic transition energies, and crystallographic data for **1a**. This material is available free of charge via the Internet at http://pubs.acs.org.

IC7023692

(56) For further details, see: Collini, M.; Chirico, G.; Baldini, G.; Bianchi, M. E. *Biopolymers* **1995**, *53*, 227–239.

(57) (a) Called PBE1PBE in Gaussian. Adamo, C.; Barone, V. *J. Chem. Phys.* **1999**, *111*, 6158–6170. (b) Perdew, J. P.; Burke, K.; Ernzerhof, M. *Phys. Rev. Lett.* **1996**, *77*, 3865–3868. (c) Perdew, J. P.; Burke, K.; Ernzerhof, M. *Phys. Rev. Lett.* **1997**, *78*, 1396.

(58) Kestner, N. R.; Combariza, J. E. In *Reviews in Computational Chemistry*; Lipkowitz, K. B., Boyd, D. B., Eds.; Wiley-VCH: New York, 1999; *Vol. 13*, pp 99−132.

(59) Rappé, A. K.; Casewit, C. J.; Colwell, K. S.; Goddard, W. A., III; Skid, W. M. *J. Am. Chem. Soc.* **1992**, *114*, 10024–10035.

(60) (a) Barone, V.; Cossi, M. *J. Phys. Chem. A* **1998**, *102*, 1995–2001. (b) Cossi, M.; Barone, V. *J. Chem. Phys.* **2001**, *115*, 4708–4717. (c) Cossi, M.; Rega, N.; Scalmani, G.; Barone, V. *J. Comput. Chem.* **2003**, *24*, 669–681.

(61) *Gaussian 03*, rev. C.02; Gaussian Inc., Wallingford, CT, 2004.